Stable hydrosol prepared by deaggregation from laser synthesis nanodiamond

Aleksandr E. Aleksenskii, Marina V. Baidakova, Andrey D. Trofimuk, Biligma B. Tudupova,
Anastasia S. Chizhikova, Aleksandr V. Shvidchenko

Division of Solid State Electronics, Ioffe Institute, St. Petersburg, Russia

Corresponding author: Aleksandr E. Aleksenskii, blin@mail.ioffe.ru

ABSTRACT The new applications of nanodiamond in biology and nuclear physics require the use of products with a low content of impurities. One of the possible methods for obtaining a high-purity nanodiamond is the recently developed laser synthesis method. The aim of this work was to study the state of aggregation of laser synthesis nanodiamond particles in aqueous suspensions and to test the possibility of deaggregation of laser nanodiamond. The process of deaggregation of a laser synthesis nanodiamond is investigated. It was shown that the previously described process of deaggregation by milling with baking soda and the usual process of deaggregation give almost the same results. A solid phase from a colloidal solution of a laser synthesis nanodiamond has been isolated and investigated. The low content of impurities in the studied product was confirmed (less than 0.1% at.), the Raman, IR, and EPR spectra were studied.

KEYWORDS nanodiamonds, nanoparticles, optical properties, surface groups, EPR

1. Introduction

It is well known that nanodiamond is a product with a very wide range of applications [1]. However, in recent years, several new products based on nanodiamonds have appeared.

First of all, in the field of medical technology development, the possibility of using a detonation nanodiamond (DND) in MRI as a contrast agent has been practically demonstrated [2, 3] and as a component of the intracellular delivery system of the antiviral agent si-RNA (including in vivo) [4]. For such applications, the issue of developing a technology for obtaining a pharmaceutical-grade nanodiamond that meets Good Manufacturing Practice (GMP) requirements has become relevant. For injectable forms of medication, the content of metal contaminants should be no more than $1 \cdot 10^{-4}$ – $1 \cdot 10^{-8}$ at.%.

The use of nanodiamond for cooling and neutron reflection looks rather unexpected [5–7]. To be used as a special material in the atomic field, a product with zero content of impurities which absorb neutrons (B, Cd, Gd and other lanthanides, Co) is required.

Traditionally, the most commonly used type of nanodiamonds is detonation nanodiamond. This product is obtained by detonating explosive charges under special conditions and then separating the product from the detonation soot by the oxidizing method. Upon production of detonation nanodiamond, detonation soot is contaminated by erosion products of the explosive chamber material [12], the process of oxidative cleaning of nanodiamond is associated with contamination of the final product with heavy metals or corrosion products of reaction equipment. For this reason, conventional industrial detonation nanodiamond contains 0.5 – 1.0 % of ash-forming impurities. The most advanced cleaning methods make it possible to obtain an almost ash-free product, however, such processes are technologically quite complex and require the consumption of a large number of chemical reagents of a high degree of purification (Electronic Grade).

As a result, the question of the possibility of developing new methods for the synthesis of nanodiamonds that ensure the production of a high purity product directly in the synthesis process is relevant. One of such promising methods is recently developed method for obtaining nanodiamonds by inertial (laser) synthesis [13]. The method is based on laser ablation of a specially prepared target that containing soot and a hydrocarbon binder under a layer of optically transparent

liquid. Synthesized nanodiamond (laser nanodiamond, LND) was separated by flotation in deionized water [14, 15]. This method does not require the removal of the non-diamond component, since the resulting product does not contain a significant amount of non-diamond carbon. Recently, information has also been published on the synthesis of nanodiamonds directly in a deaggregated form when irradiated with a femtosecond laser with ethanol [16] and liquid carbon monoxide CO [17], but at present these technologies seem not might to be used for industrial scale production.

A serious advantage of the laser synthesis process is the exclusion of the use of explosives, which are not freely available reagents and require special permits, equipped facilities for storage and processing, as well as a special order of transportation.

For many applications, it is extremely important to obtain nanodiamond in the form of a colloidal solution containing individual free particles. In the form of a colloidal solution, nanodiamonds can be relatively easily cleaned and subjected to various chemical modifications.

In recent paper [18], Stehlik and co-authors reported successful deaggregation of a laser nanodiamond by obtaining a colloidal solution of free particles with a negatively charged surface by a method developed by Mochalin [19]. The method is based on ultrasonic processing of the initial nanodiamond in a NaCl or NaHCO$_3$ slurry. At the same time, before ultrasonic treatment, the source material is processed in the same way as previously described [9] or [10]. For this reason, there are reasonable doubts about the need to use salt slurry.

The aim of this work was to study the state of nanodiamond particles obtained by laser synthesis in aqueous suspensions and to test the possibility of obtaining nanodiamond colloids of this type consisting of free particles without the use of slurry of soluble salts and operations associated with this method. We also investigated the properties of such solutions, isolated a solid product from a colloidal solution, conducted a primary assessment of the purity of the resulting product and investigated some practically important physical properties.

2. Experimental

The laser nanodiamond (LND) sample was obtained by laser ablation of a target containing industrial carbon black and a hydrocarbon binder with the addition of stearic acid under a layer of water. A pulsed solid-state YAG laser with a wavelength of 1064 nm was used for irradiation. The synthesized LND was separated by flotation, additionally washed and dried. A more complete description of the synthesis is given in [13].

We used the deaggergation procedure similar to that previously described in [9]. The powder of the LND 7.5 g mass was placed in a graphite boat, which was installed in a quartz tube with a heater blown by a flow of hydrogen. The treatment temperature was 600 °C, the hydrogen treatment time was 6 hours. After cooling the product was mixed with 200 ml of deionized water and sonicated for 15 minutes (the temperature increase was 30 °C). After sonication, the product was separated by centrifugation (RCF $1.8 \cdot 10^4$ g), while a gray (sometimes bright blue or light blue, the origin of this color is the subject of discussion) precipitate and a black color supernatant were formed. Sonication of precipitate in water and centrifugation of obtained colloidal solution were repeated three times, as a result, 500 ml of a black supernatant were obtained.

The DND sample for ESR measurement was obtained from an industrial nanodiamond manufactured by SKTB "Technolog". The product was purified by washing with hydrochloric and hydrofluoric acid, annealed in hydrogen at 600 °C, sonicated and separated by centrifugation in accordance with [9]. The solid phase was separated by a vacuum rotary evaporator.

LND particle sizes were measured using a Mastersizer 2000 laser diffraction analyzer (Malvern Instruments, UK) and a LiteSizer 500 nanoparticle analyzer (Anton Paar, Au). The same device was used to measure the electrokinetic potential (PALSE).

X-ray diffraction (XRD) data were obtained using a powder diffractometer D2 Phaser (Bruker AXS, Germany) designed in vertical Bregg–Brentano θ–θ geometry and equipped with semiconductor linear position-sensitive detector LYNXEYE with opening angle of 5°. The measurements were performed in symmetric θ–2θ scan mode using Cu-Kα radiation monochromatized by Ni filter. To average the effect of preferred crystallite orientation, the sample was rotated around the sample holder axis coinciding with the axis of the diffractometer goniometer. To avoid the diffraction contribution of the sample holder and the adhesive, the samples were mounted on a background-free holder in the form of the Si(119) single crystal wafer. XRD patterns were analyzed using the TOPAS-5 program using the Scherrer model.

The Raman spectra were obtained using the Ntegra Spectra spectrometer (SOL Instruments, NT-MDT, Ru). A 532.01 nm diode laser (Integrated Optics) was used. To prevent heating of the sample, the radiation power density did not exceed $2 \cdot 10^3$ W/cm^{-2}. Diffraction gratings 600/600 bar/mm were used. All measurements were carried out at room temperature.

IR spectra were recorded using an Infralum FT-08 Fourier spectrometer (Lumex, Ru). To register the spectrum, 200 measurements were made with a resolution of 2 cm^{-1}.

Elemental analysis was performed using TESCAN VEGA-3 SBH SEM with an INCA X-act X-ray energy analyzer (Oxford Instruments, UK). The average variation for each channel is no more than 0.5 %.

EPR spectra were obtained using the ESR 70-03 XD/2 (KBS, Be) 9 GHz band (X-band) with a maximum generator power of 0.8 W. (microwave attenuation of 22 dB), modulation amplitude of 0.1 mT, number of signal accumulations

of 1, total spectrum recording time for one pass was 100 s. For quantitative measurements, short quartz tubes on a Teflon holder were used.

Sonication was performed using a UZG4-1.0/22 generator with magnetostrictive transducer with titanium alloy horn on frequency of 22 kHz. The acoustic power measured by the calorimetric method was 35 W.

Particle separation was performed on a Sigma 6-16 centrifuge with a 12169 rotor equipped with a set of Sarstedt capsules #0037-109.4827.

3.   Results and discussion

The studied sample of nanodiamond looked initially as a gray powder. Its properties are described in more detail in [15]. To study the particle size distribution, the sample of the initial powder weighing 15 mg was mixed with 150 ml of water and sonicated for 15 minutes with 5 Wt power. The particle size distribution measured after cooling the sample is shown in Fig. 1.
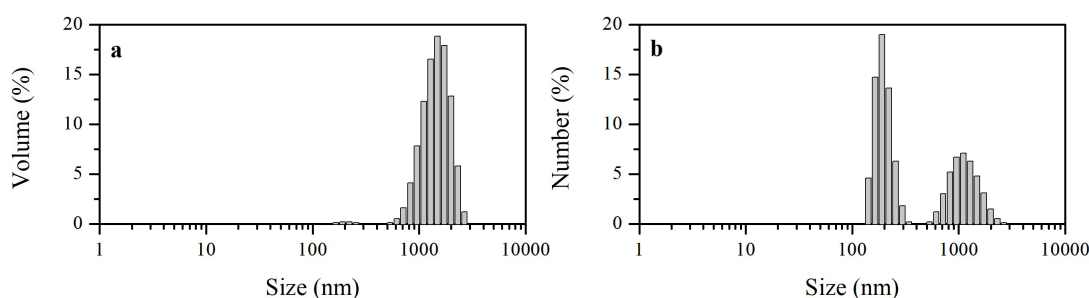

FIG. 1. The distribution of LND particles in water suspension after sonication by volume (a) and by the number of particles (b). Data was determined by the DLS

According to the results of measurements using DLS, it was found that most of the particles have a size of about 1 micron, but there is a significant proportion of particles with a smaller diameter (200 nm). Similar results were obtained when measuring the particle distribution by laser diffraction (Fig. 2). The distribution peaks are slightly shifted relative to the results of DLS measurements (220 and 2000 nm, respectively).
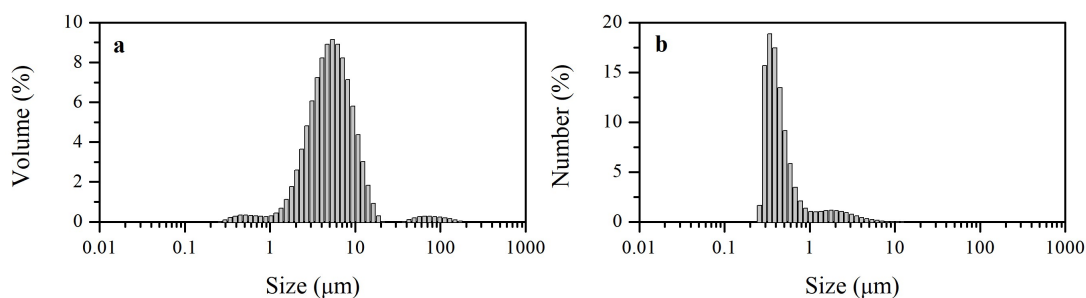

FIG. 2. The distribution of LND particles in water suspension after sonication by volume (a) and by the number of particles (b). Data was determined by the laser diffraction (Mastersizer 2000)

To explore the possibility of obtaining a colloidal solution containing single nanodiamond particles, we used the deaggergation procedure similar to that previously described by Williams et al [9].

The particles size distribution by volume in the obtained black colloidal solution, determined by the DLS, is shown in Fig. 3. Based on these results, we can conclude that the formation of a colloidal solution of LND is similar to the previously described [9].

When the produced solution was evaporated, it was possible to obtain a solid phase. The concentration of produced suspension was approximately 0.8 % by weight. Thus, the total yield of the solid phase was about 50 % of the initial mass of nanodiamond, which is quite close to that claimed by Stehlik [18].

An XRD pattern of the isolated solid product confirmed that the dispersed phase is the diamond (Fig. 4). According to the phase analysis, all the intense reflections observed in the XRD patterns of all samples correspond to the C cubic crystal (diamond phase, space group Fm3 (227), $\alpha = 3.56637$ Å at room temperature) [19]. All possible diamond reflections are observed; therefore, the samples are polycrystalline with crystallites about 4 nm in size (the crystallite sizes D obtained in the model without microstrains ($\varepsilon s = 0$)). A thorough analysis of the XRD reflection profiles of the sample by the TOPAS methods has shown that the broadening of reflections is caused not only by the crystallite size D but also arises
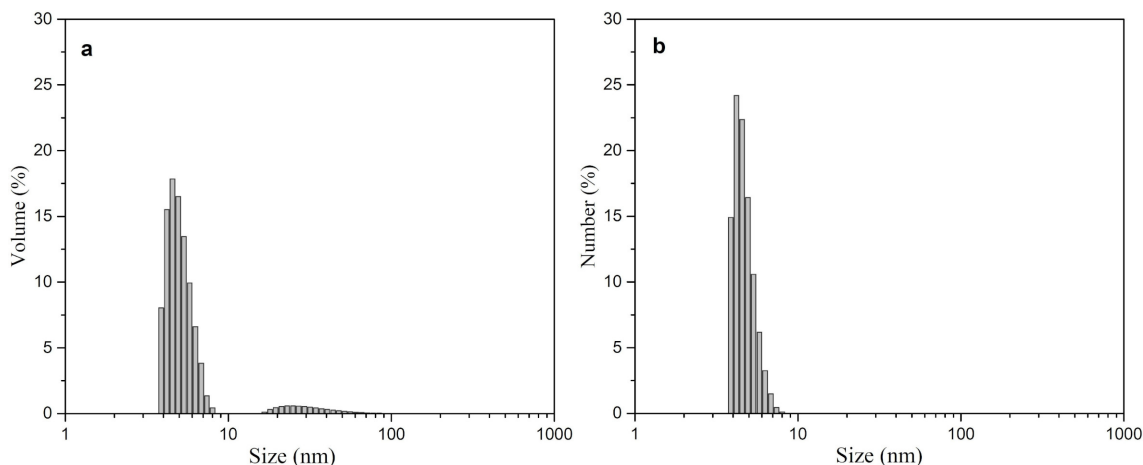
FIG. 3. The particle size distribution by volume (a) and by the number (b) of LND particles in supernatant water after deaggregation procedure. Data was determined by the DLS

due to microdeformations εs in them. The mean values of D obtained in the model with non-zero εs are characterized by slightly lower standard deviations than those calculated using the $\varepsilon s = 0$, but both methods give comparable values that agree well within one e.s.d. ($D = 4.50(4)$ and $4.34(4)$ nm, respectively). Also it should be noted the change of the observed preferred orientation along the (111) direction, which is typical for a powder of isolated diamond nanoparticles and was previously mentioned in the literature [10].
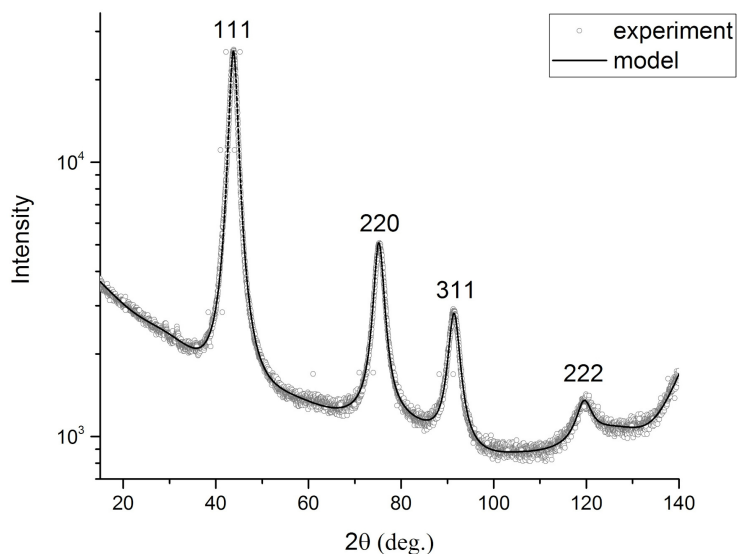

FIG. 4. Model and experimental XRD patterns of the isolated solid product. The Miller indices hkl of the reflections of the observed crystalline diamond phases are indicated

The results of particle size measurements performed by the DLS method and the value of the crystal size obtained by processing X-ray diffraction data coincide well. This suggests that we have produce a colloidal solution containing free nanodiamond particles.

The Raman spectrum of the isolated solid product (Fig. 5) has a form similar to that of the Raman spectrum of a deaggregated DND obtained by similar procedure described in [9]. It has the same characteristic features: some displacement of the peak center relative to a massive diamond and broadening of the spectrum lines. Moreover, the diamond peak maximum located at 1326 cm^{-1}, which corresponds to 4 nm particles by phonon confinement model (described at [23]). Note that there is some discrepancy between the X-ray data and the Raman spectrum. While there are no signs of the presence of graphite phase residues on the X-ray of the LND, in the Raman spectrum of the LND, the ratio of the diamond and G-peak is noticeably smaller compared to the spectrum of the DND.

Figure 6 shows the IR spectra of the sample of deaggregated LND in comparison with a sample of a deaggregated DND. The structure of the spectra is repeated, except for a narrow peak of 1394 cm^{-1}, which is absent in the spectrum of the LND.
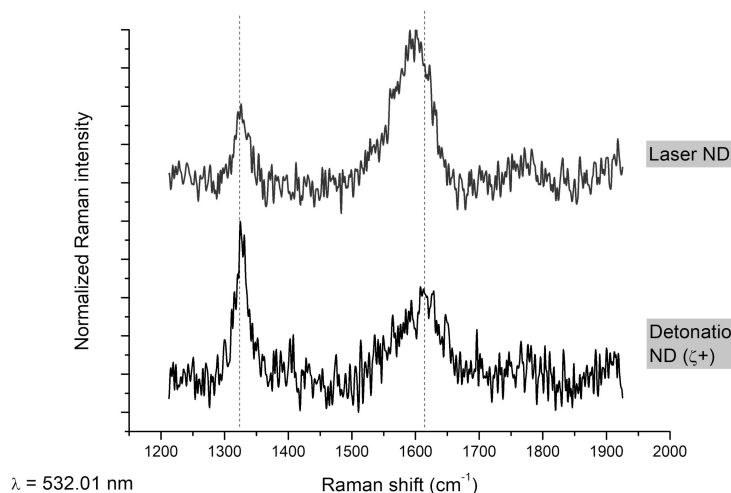
FIG. 5. The Raman spectrum of a deaggregated LND. For comparison, the Raman spectrum of a deaggregated DND is given
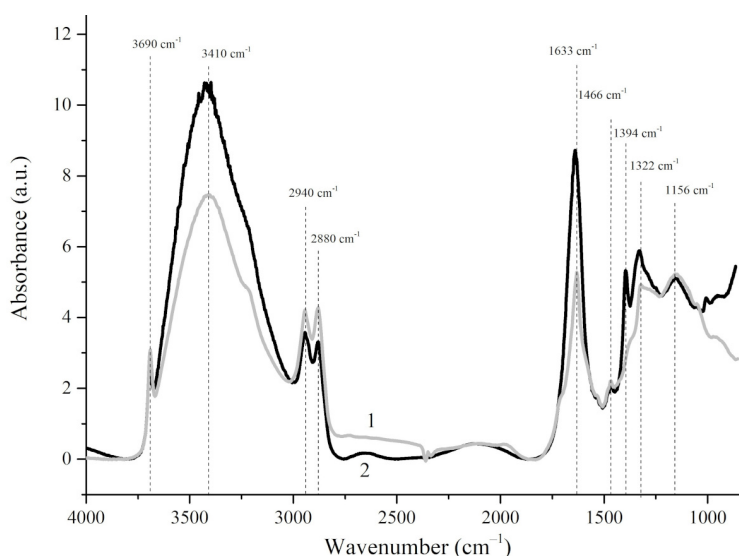

FIG. 6. IR spectra of deaggregated LND (1) and deaggregated DND (2)

The presence of a wide band with a maximum at 3410 cm^{-1} and a narrow band with a maximum at 3690 cm^{-1} corresponds to the valence vibrations of the O–H bond, mainly water sorbed by the sample itself. A narrow band with a peak in the region of 1636 cm^{-1} refers to deformation vibrations of O–H. Bands in the regions of 2960, 2880, 1466 cm^{-1} correspond to valence vibrations of methyl and methylene groups (–CH$_3$, –CH$_2$). The peak in the region of 1322 cm^{-1} characterizes the valence oscillations of C–C in diamond. Fluctuations of C–O belonging to lactones or esters are manifested in the region of 1156 cm^{-1}.

Comparison of the spectra shows that samples of diamond nanoparticles by the laser and the detonation synthesis have similar composition of functional groups on the surface. The main difference is that the peak in the 1394 cm^{-1} region corresponding to the C–O valence oscillations is not presented in the spectrum of the laser synthesis sample.

As has been repeatedly noted, the deaggregated DND, which after hydrogen treatment contains methyl and other groups with C–H bonds, is characterized by a positive surface charge with an electrokinetic potential of 40 – 50 mV. A similar pattern is observed for laser synthesis nanodiamond after treatment in hydrogen. The measured value of the electrokinetic potential was about +45 mV.

The elemental composition of the LND was studied by the energy-dispersive X-ray spectroscopy (EDS) method. A typical EDS spectrum is shown in Fig. 7, the corresponding impurity content estimate is given in the upper right. A more accurate analysis result is shown in Table 1.

The content of the most impurity elements in the studied sample is at the noise level and corresponds to well-purified samples of DND. Attention is drawn to the low nitrogen content, which is usually much higher for DND – about 4 % or more [20]. However it is not zero at all as expected. This fact is presumably due to the laser synthesis in the air
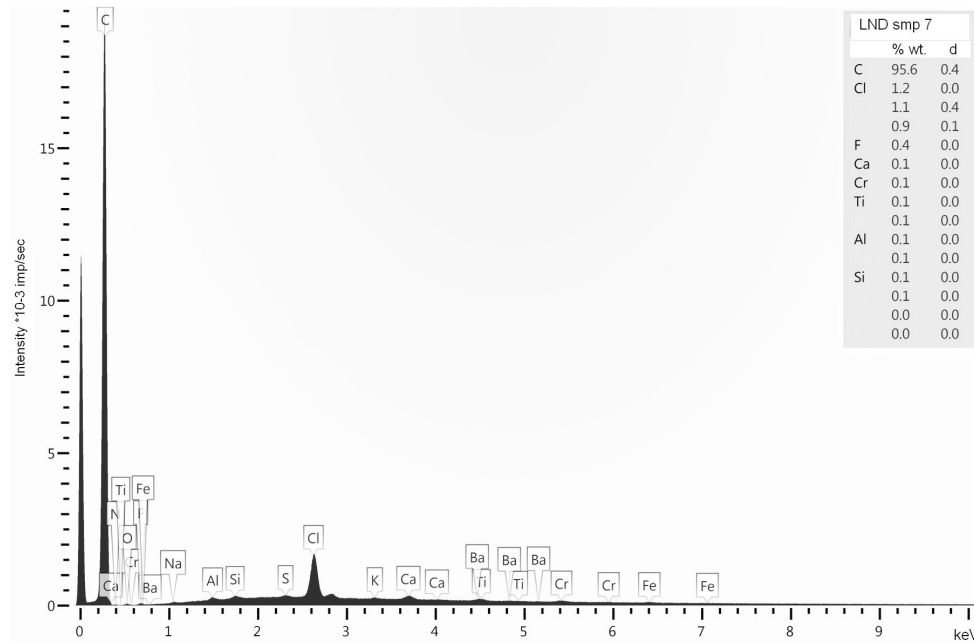
LND smp 7		
	% wt.	d
C	95.6	0.4
Cl	1.2	0.0
	1.1	0.4
	0.9	0.1
F	0.4	0.0
Ca	0.1	0.0
Cr	0.1	0.0
Ti	0.1	0.0
	0.1	0.0
Al	0.1	0.0
	0.1	0.0
Si	0.1	0.0
	0.1	0.0
	0.0	0.0
	0.0	0.0

FIG. 7. Results of EDS analysis of deaggregated LND

TABLE 1. Element composition of LND sample

	C	N	O	F	Na	Al	Si	S	Cl	K	Ca	Ti	Cr	Fe	Ba
mass.%	95.59	1.15	0.91	0.44	0.06	0.07	0.05	0.05	1.23	0.04	0.13	0.08	0.09	0.05	0.08
at.%	97.38	1.00	0.69	0.29	0.03	0.03	0.02	0.02	0.42	0.01	0.04	0.02	0.02	0.01	0.01

atmosphere. In this case the air dissolved in the water used is captured. It is also possible to capture atmospheric nitrogen directly during synthesis due to the intensive mixing. Obviously the result can be improved by blowing of the argon and providing the laser synthesis in a nitrogen-free atmosphere. We should also hope for a significant reduction in the content of impurities during laser synthesis under conditions corresponding to GMP.

The measured EPR spectrum has no significant differences from the EPR spectrum of the detonation nanodiamond (Figs. 8, 9). There is no splitting of the single intense line. The concentration of paramagnetic centers in the LND sample is slightly higher (approximately 105 %) of the concentration of paramagnetic centers ($5.0 \cdot 10^{18}$ units/g) in the reference sample of detonation nanodiamond.
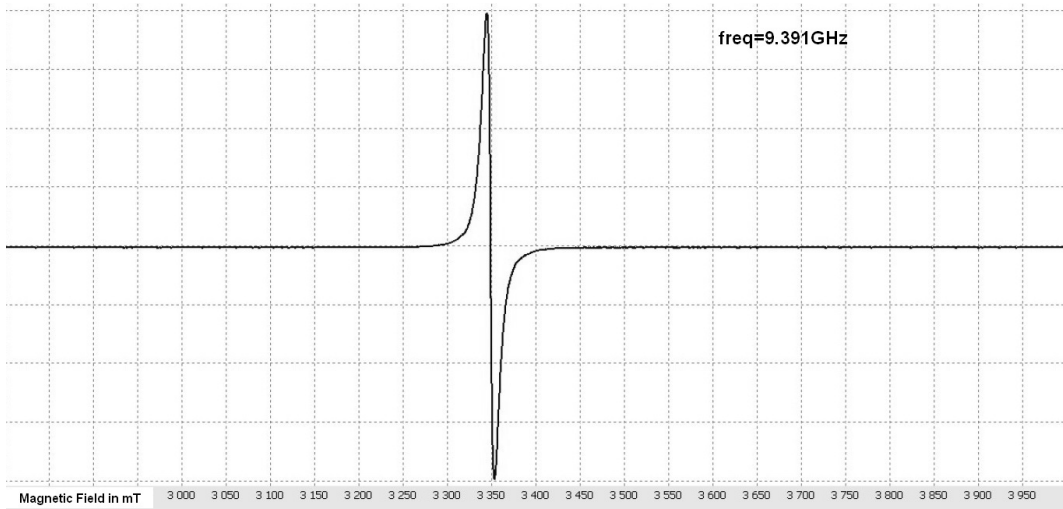

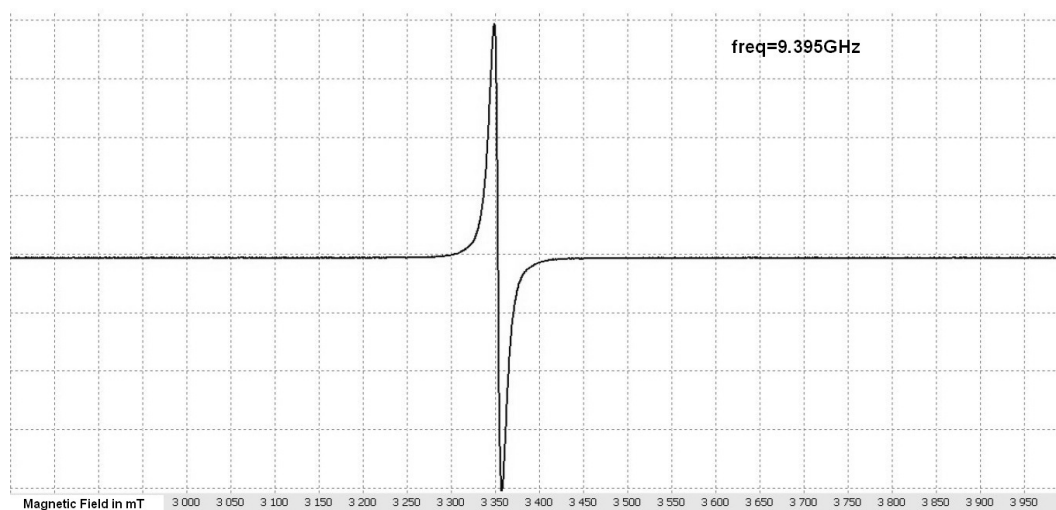FIG. 8. EPR spectrum of deaggregated LND. Sample mass is 5.9 mg

FIG. 9. EPR spectrum of deaggregated DND with positive surface charge. Sample mass is 6.2 mg

For the purpose of preliminary evaluation of the relaxivity of the resulting product spectra with high power input 200 and 400 mW were measured. There was not found the significant change in the shape of the lines or signal suppression. This suggests a potentially high spin-spin interaction constant, which is needed for the use of nanodiamond in contrast agents for MRI. Of course, the correct measurement of the relaxivity of a deaggregated LND will be the subject of the next article.

4. Conclusions

1. The aggregation of nanodiamond particles by laser synthesis in aqueous suspensions is investigated. It has been established that nanodiamonds are contained in aggregates ranging in size from 200 nm to 1 μm depending on modifications of the synthesis conditions. Nanometer particles of the laser nanodiamond were not detected in the pristine product.
2. The process of deaggregation of the laser synthesis nanodiamond is investigated. The colloidal solution of LND with a positive surface charge containing free nanodiamond particles of about 5 nm in size was obtained.
3. The output of the deaggregated product is nearly to the previously described process using salt slurry. The need for its use is not obvious, thus the use of salt slurry is, apparently, a "successful complication" of the deaggregation procedure, because of the fact that the use of additional reagents of inadequate quality can cause contamination of the final product.
4. The solid phase from the colloidal solution of laser nanodiamond is isolated and investigated, its diamond nature is confirmed. The low content of impurities in the investigated product was confirmed.
5. The EPR spectra of the deaggregated laser synthesis nanodiamond has been studied. The parameters of the EPR signal are close to those for the detonation synthesis nanodiamond, which suggests the possibility of its use in relaxation agent for MRI.

References

[1] Dideikin A. *Applications of Detonation Nanodiamonds in Detonation Nanodiamonds: Science and Applications*. Jenny Stanford Publishing, Singapore, 2014, 346 p.
[2] Panich A., Salti M., Prager O., Swissa E., Kulvelis Yu., Yudina E., Aleksenskii A., Goren Sh., Vul' A., Shames A. PVP-coated Gd-grafted nanodiamonds as a novel and potentially safer contrast agent for in vivo MRI. *Magn Reson Med.*, 2021. 8, P. 1–8.
[3] Panich A., Shames A., Aleksenskii A., Yudina E., Vul A.Ya. Manganese-grafted detonation nanodiamond, a novel potential MRI contrast agent. *Diamond & Related Materials*, 2021, 119, 108590
[4] Jingru Xu, Mengjie Gu, Lissa Hooi, Tan Boon Toh, Dexter Kai Hao Thng, Jhin Jieh Limb, Edward Kai-Hua Chow. Enhanced penetrative siRNA delivery by a nanodiamond drug delivery platform against hepatocellular carcinoma 3D models. *Nanoscale*, 2021, 13, 16131
[5] Artem'ev V. Estimation of neutron reflection from nanodispersed materials. *At. Energy*, 2006, 101, P. 901–904.
[6] Nesvizhevsky V., Lychagin E., Muzychka A., Strelkov A., Pignol G., Protasov K. The reflection of very cold neutrons from diamond powder nanoparticles. *Nucl. Instrum. Methods*, 2008, 595, P. 631–636.
[7] Aleksenskii A., Bleuel M., Bosak A., Chumakova A., Dideikin A., Dubois M., Korobkina E., Lychagin E., Muzychka A., Nekhaev G., et al. Clustering of Diamond Nanoparticles. Fluorination and Efficiency of Slow Neutron Reflectors. *Nanomaterials*, 2021, 11, 1945.
[8] Kruger A., Kataoka F., Ozawa M., Fujino T., Suzuki Y., Aleksenskii A., Vul' A., Osawa E. Unusually tight aggregation in detonation nanodiamond: Identification and disintegration. *Carbon*, 2005, 43 (8), P. 1722–1730.
[9] Williams O., Hees J., Dieker C., Jager W., Kirste L., Nebel C. Size-Dependent Reactivity of Diamond Nanoparticles. *ACS Nano*, 2010, 4 (8), P. 4824–4830.
[10] Aleksenskiy A., Eydelman E., Vul'A. Deaggregation of Detonation Nanodiamonds. *Nanosci. Nanotechnol. Lett.*, 2011, 3, P. 68–74.

[11] Aleksenskii A., Kirilenko D., Trofimuk A., Shvidchenko A., Yudina E. Deaggregation of polycrystalline diamond synthesized from graphite by shock-compression. *Fullerenes, Nanotubes and Carbon Nanostructures*, 2021, 29 (10), P. 779–782.

[12] Aleksenskii A. *Technology of preparation of detonation nanodiamond in Detonation Nanodiamonds: Science and Applications*, Jenny Stanford Publishing, Singapore, 2014, 346 p.

[13] Perevedentseva E., Peer D., Uvarov V., Zousman B., Levinson O. Nanodiamonds of Laser Synthesis for Biomedical Applications. *J. of Nanoscience and Nanotechnology*, 2015, 15, P. 1045–1052.

[14] Panich A., Shames A., Zousman B., Levinson O. Magnetic resonance study of nanodiamonds prepared by laser-assisted technique. *Diamond & Related Materials*, 2012, 23, P. 150–153

[15] Baidakova M., Kukushkina Yu., Sitnikova A., Yagovkina M., Kirilenko D., Sokolov V., Shestakov M., Vul' A., Zousman B., Levinson O. Structure of Nanodiamonds Prepared by Laser Synthesis. *Physics of the Solid State*, 2013, 55 (8), P. 1747–1753.

[16] Nee C.-H., et al. Direct synthesis of nanodiamonds by femtosecond laser irradiation of ethanol. *Nature Sci. Rep.*, 2016, 6, 33966.

[17] Armstrong M., Lindsey R., Goldman N., Nielsen H., Stavrou E., Fried L., Zaug J., Bastea S. Ultrafast shock synthesis of nanocarbon from a liquid precursor. *Nature Comm.*, 2020, 11, 353.

[18] Stehlik S., Henych J., Stenclova P., Kral R., Zemenova P., Pangrac J., Vanek O., Kromka A., Rezek B. Size and nitrogen inhomogeneity in detonation and laser synthesized primary nanodiamond particles revealed via salt-assisted deaggregation. *Carbon*, 2021, 171, P. 230–239.

[19] Mochalin V., Turcheniuk K., Trecazzi C., Deeleepojananan C. Salt-Assisted Ultrasonic Deaggregation of Nanodiamond. *ACS Appl. Mater. Interfaces*, 2016, 8, P. 25461–25468.

[20] Topas Version 5. Technical reference. Brucker AXS, Karlsruhe, Germany, 2014. URL: https://www.bruker.com/en/products-and-solutions/diffractometers-and-scattering-systems/x-ray-diffractometers/diffrac-suite-software/diffrac-topas.html

[21] Hom T., Kiszenik W., Post B. Accurate lattice constants from multiple reflection measurements. II. Lattice constants of germanium silicon, and diamond. *J. Appl. Cryst.*, 1975, 8, P. 457–458.

[22] Shenderova O., Vlasov I., Turner S., Gustaaf Van Tendeloo, Orlinskii S., Shiryaev A., Khomich A., Sulyanov S., Jelezko F., Wrachtrup J. Nitrogen Control in Nanodiamond Produced by Detonation Shock-Wave-Assisted Synthesis. *J. Phys. Chem. C*, 2011, 115, P. 14014–14024.

[23] Meilakhs A., Koniakhin S. New explanation of Raman peak redshift in nanoparticles. *Superlattices Microstruct.*, 2017, 110, P. 319–323.

Information about the authors:

Aleksandr E. Aleksenskii – Division of Solid State Electronics, Ioffe Institute, Polytechnicheskaya 26, 194021 St. Petersburg, Russia; ORCID 0000-0002-5004-6993; blin@mail.ioffe.ru

Marina V. Baidakova – Centre of Nanoheterostructure Physics, Ioffe Institute, Polytechnicheskaya 26, 194021 St. Petersburg, Russia; ORCID 0000-0002-5524-7233; baidakova@mail.ioffe.ru

Andrey D. Trofimuk – Division of Solid State Electronics, Ioffe Institute, Polytechnicheskaya 26, 194021 St. Petersburg, Russia; ORCID 0000-0003-3140-0245; trofimuk.ad@mail.ioffe.ru

Biligma B. Tudupova – Division of Solid State Electronics, Ioffe Institute, Polytechnicheskaya 26, 194021 St. Petersburg, Russia; ORCID 0000-0002-7655-294X; biligma0201@gmail.com

Anastasia S. Chizhikova – Division of Solid State Electronics, Ioffe Institute, Polytechnicheskaya 26, 194021 St. Petersburg, Russia; ORCID 0000-0002-0120-5847; chizhikova@mail.ioffe.ru

Aleksandr V. Shvidchenko – Division of Solid State Electronics, Ioffe Institute, Polytechnicheskaya 26, 194021 St. Petersburg, Russia; ORCID 0000-0002-5417-7472; avshvid@mail.ioffe.ru

Conflict of interest: the authors declare no conflict of interest.